ISBN: 978-3-95450-247-9 ISSN: 2673-5490 doi: 10.18429/JACoW-IPAC2024-TUAD2

CORRECTING ASYMMETRY OF CLOSED-ORBIT DISTORTION IN J-PARC MAIN RING BY REDUCING CURRENT RIPPLES OF MAIN MAGNET POWER SUPPLIES

Y. Morita[1†], Y. Tan, M. Yoshii[1], H. Hotchi[1], S. Igarashi[1], K. Miura, T. Yasui[1], T. Shimogawa[1], T. Asami, Y. Sato[1], KEK, Tokai, Japan
M. Yoshinari, NAT Corporation, Tokai, Japan
R. Sagawa, Universal Engineering, Mito, Japan
[1]also at SOKENDAI, Tokai, Japan

Abstract

The magnet power supply system of the main ring in the Japan proton accelerator research complex (J-PARC) was upgraded to increase the beam power for T2K long-baseline neutrino experiment. However, the asymmetric fluctuation of the closed orbit was observed after the upgrade. The cause of the asymmetry was attributed to the large ripples of the excitation currents for the bending magnets. The measures to reduce the ripples were applied to six identical power supplies for the bending magnets, and then the asymmetry was successfully corrected.

INTRODUCTION

The power supplies for the bending magnet (BM) families have been replaced with the new power supplies that were developed for the high repetition rate operation of the main ring (MR) in the Japan proton accelerator research complex (J-PARC) [1]. The increase of the repetition rate of the MR cycle from 2.48 s to 1.36 s contributes to the increase of the beam power for T2K long-baseline neutrino experiment [2]. The specifications and the schematic of a single new BM power supply (BMPS) are shown in Figs. 1 and 2, respectively. Six DC/DC converters with a rated voltage of 1650 V were connected in series to achieve a rated voltage ± 5.5 kV peak. Most of the power is transferred between the capacitor banks and magnets in each MR cycle. Only resistive loss is supplied by the electrical system [3]. Six BM families in total are symmetrically arranged in the MR tunnel (Fig. 1).

After the upgrade of the magnet power supply system, a time variation of the closed orbit that breaks the three-fold symmetry of the lattice was observed. In Fig. 3, the horizontal beam positions of high dispersion positions at the interval of 1 ms are plotted with the grey curves. The individual analysis is possible for every BM family since the achromat lattice is adopted for every half arc. The amplitudes of the curves for BM1 and 2 are the largest among all BM families. The current deviations, ΔI, normalized with the flat bottom current of the BMPS that are shown in Fig. 4 with the grey curves also indicate the ripples of BM1 and 2 are the largest. The components in the frequency range of > 500 Hz were removed in Fig. 4 since the components of the magnetic field in this frequency range are expected to be negligible owing to the shielding effect of the eddy current that flows in the beam duct. All data were measured in the DC state of the flat bottom current.

The simulated beam-survival ratio decreased when the current ripples of BM and quadrupole magnet (QM) families were introduced. The results of the simulation that are shown in Fig. 5 indicate the ripples of K_0 components are the major sources of the beam loss [4]. The possible scenario of this mechanism is described as follows. The asymmetry of the closed-orbit distortion (COD) appears at the arc-sections because of the difference in the current ripples of BM families. Subsequently, the K_1 error is induced due to the coupling of the COD and K_2 components by sextupole magnets. Consequently, the three-fold symmetry is broken and the emittance increases.

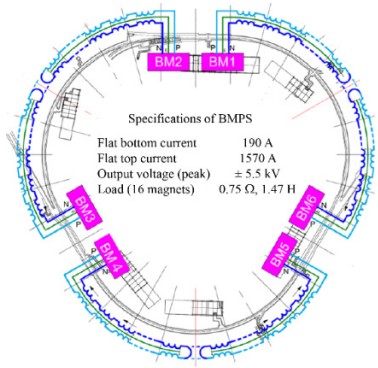

Figure 1: Specifications of the new BMPS and schematic of the arrangement of BM families.

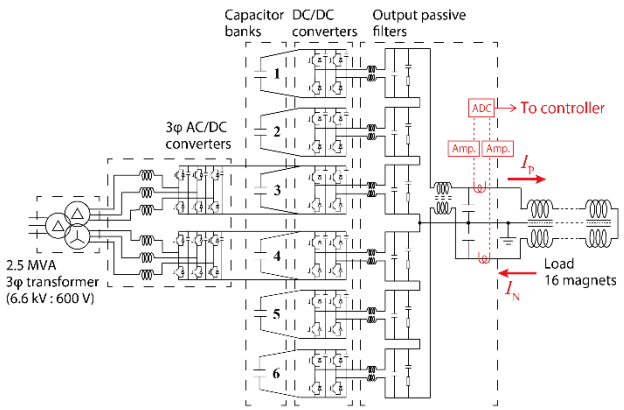

Figure 2: Schematic of BMPS. The analog signals of the current sensors for the measurement of the output currents are digitized before being transferred to the controller.

† yuichi.morita@kek.jp

ISBN: 978-3-95450-247-9 ISSN: 2673-5490 doi: 10.18429/JACoW-IPAC2024-TUAD2

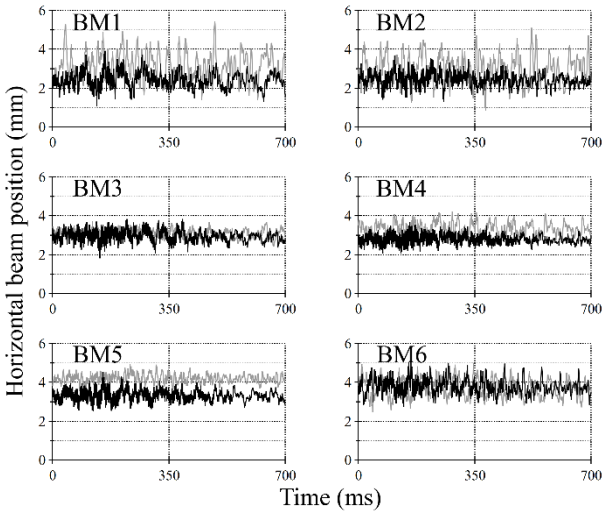

Figure 3: Horizontal beam positions of high dispersion positions at the interval of 1 ms. The grey and black lines represent the waveforms before and after the improvement.

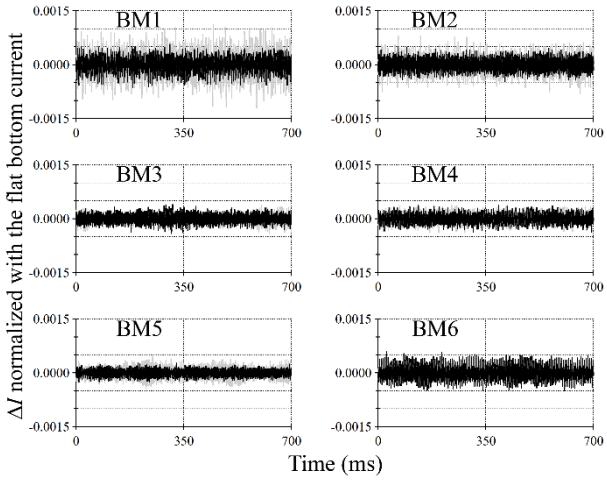

Figure 4: Normalized ΔI of BM families. The grey and black lines represent the waveforms before and after the improvement.

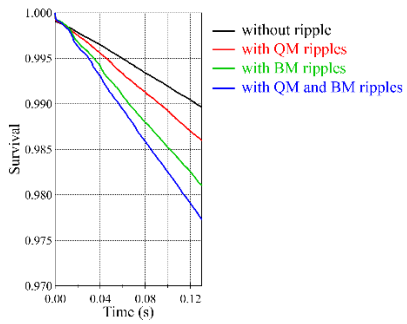

Figure 5: Simulated beam-survival ratio including the effect of the current ripples of BM and QM.

EXPERIMENTAL

The investigation of the source of the current ripples focuses on the analog signals before the digitization since the impact of the noise on the digital signal is less than that on the analog signal. In the new power supply, all analog signals of current and voltage sensors are digitized with the analog-to-digital converter (ADC) boards. Then, only digital signals are transferred to the controller through the optical cables to electrically isolate the controller from the main circuit [5].

DC Current Transformer (DCCT)

The influence of the external magnetic field on the analog signals of the DCCT system was investigated. The specifications of the DCCT that is installed in the BMPS are listed in Table 1. Two identical DCCTs are used to measure the output currents of I_P and I_N in a single BMPS. The definitions of I_P and I_N are depicted in Fig. 2. The mean value of I_P and I_N is used for the feedback value of the current control to cancel the common mode ripple current [6]. The structures around the DCCT heads are shown in Fig. 6. The distance between the two heads is approximately 450 mm. The busbar of the ground line is centrally positioned between the two DCCT heads.

The current that flows in the ground line is one possible source of the noise on ΔI. The measured current deviation of the ground line is approximately ± 70 A_{peak} in the DC state of the flat bottom current though that of I_P or I_N are approximately only ± 1 A_{peak}. The investigation focuses on the relationship between the DCCT head and the current of the ground line since the external magnetic field generally have to be minimized to reduce the influence on the DCCT signals [7].

Table 1: Specifications of DCCT

Output	Current output
Burden resistor	1 Ω
Rated current	2000 A
Current transfer ratio	2000 : 1

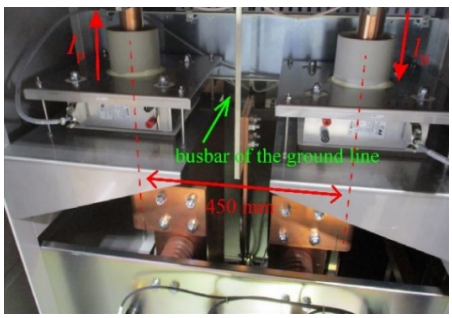

Figure 6: Structures around DCCT heads.

Distance Dependency

ΔI as a function of the distance between the DCCT head and the conducting wire was measured to survey the influence of the magnetic field on the DCCT head. As is shown in Fig. 7 (left), the DCCT head is removed from the power supply, and then, placed nearby the prepared wire. The waveform of the current in the wire is plotted in Fig. 8 (left). The root-mean-squared (RMS) ΔI are plotted in Fig. 8 (right). The triangle and the inverted triangle represent the result of the DCCT head for I_P and I_N, respectively. When one DCCT head is examined, the input of the ADC board

ISBN: 978-3-95450-247-9 ISSN: 2673-5490 doi: 10.18429/JACoW-IPAC2024-TUAD2

for the other DCCT head is shorted. The calculated RMS magnetic field that is generated by the current that flows in the prepared wire is also plotted. The magnetic flux density, B, is calculated as

$$B = \frac{\mu_0 I}{2\pi R}. \quad (1)$$

where μ_0, I, and R represent the permeability of the air, RMS current in the prepared wire, and the distance between the centre of the DCCT head and the wire, respectively.

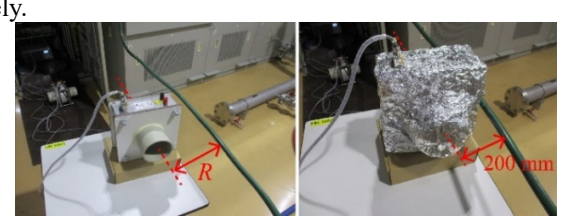

Figure 7: Experimental setup for distance dependency (left) and shield dependency (right).

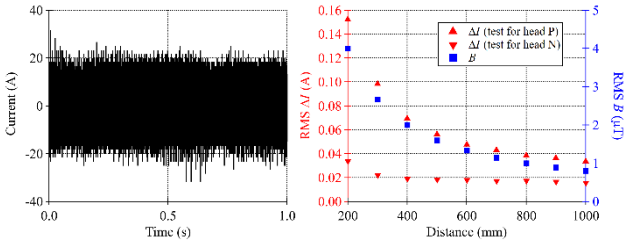

Figure 8: Current that flows in the prepared wire (left). RMS ΔI and B as a function of the distance between the DCCT head and the wire (right).

Shield Dependency

Another investigation for the impact of the magnetic field on ΔI was conducted by shielding the DCCT head. As is shown in Fig. 7 (right), one DCCT head is totally covered with the aluminium foil of 11 μm thickness. The input of the ADC board for the other DCCT head is shorted. The RMS ΔI before and after the shield are listed in Table 2. The distance between the centre of the DCCT head and the wire is fixed to 20 mm. The reduction of the noise on ΔI was observed after the shielding.

Table 2: RMS ΔI Before and After the Shield

	Head P	Head N
Before shield	0.152 A	0.029 A
After shield	0.044 A	0.019 A

CORRECTION OF COD ASSYMETRY

Two test results show the electromagnetic interference caused by the ground current is not negligible. To reduce the influence on ΔI, the existing ground line is disconnected and bypassed for all six BMPSs. As is shown in Fig. 9, the distance between the bypassed line and the DCCT heads are sufficiently increased. The horizontal beam positions and the current ripples after the bypass are plotted with the black curves in Figs. 3 and 4, respectively. The fast Fourier transforms (FFTs) of these data for BM1 and 2 are plotted in Figs. 10 and 11, respectively. The noise in ΔI of BM1 and 2 were successfully decreased in the whole frequency range. Consequently, the asymmetry of the COD was improved.

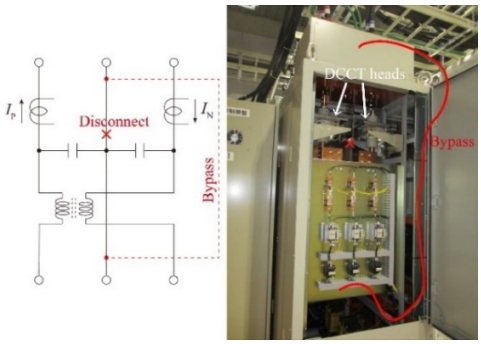

Figure 9: Schematic and picture of the bypass.

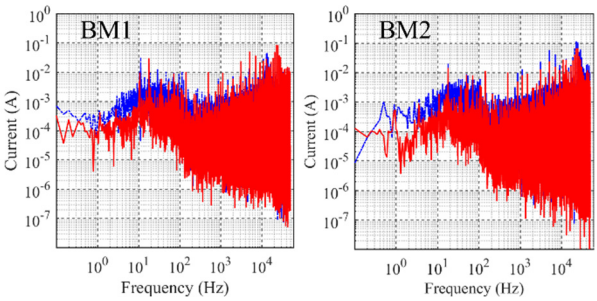

Figure 10: FFTs of ΔI for BM1 and 2. Dashed blue and solid red lines represent the waveforms before and after the improvement, respectively.

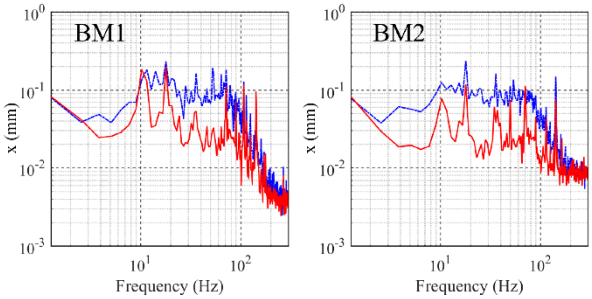

Figure 11: FFTs of the horizontal beam positions of high dispersion positions at the interval of 1 ms (average of 10 shots data). Dashed blue and solid red lines represent the waveforms before and after the improvement, respectively.

CONCLUSION

The cause of the asymmetry of BM ripples was identified as the electromagnetic interference caused by the ground current. The ground routes of BMPSs were bypassed to increase the distance between the DCCT heads and the ground line. Consequently, the asymmetric fluctuation of the closed orbit was successfully improved.

This result suggests the tune region of the stable beam operation is expected to be improved since the effect of the non-structure resonance should be suppressed.

ISBN: 978-3-95450-247-9 ISSN: 2673-5490 doi: 10.18429/JACoW-IPAC2024-TUAD2

REFERENCES

[1] Y. Morita *et al.*, "Upgrading magnet power supply system in J-PARC main ring", *Proc. IPAC'23*, Venice, Italy, May 2023. pp. 3762-3765. doi:10.18429/JACoW-IPAC2023-WEPM082.

[2] S. Igarashi *et al.*, "Accelerator design for 1.3-MW beam power operation of the J-PARC Main Ring", *Prog. Theor. Exp. Phys.* 2021, 033G01. doi:10.1093/ptep/ptab011.

[3] T. Shimogawa *et al.*, "New Power Supply of Main Magnets for J-Parc Main Ring Upgrade", *Proc. IPAC'19*, Melbourne, Australia, May 2019, pp. 1266-1268. doi:10.18429/JACoW-IPAC2019-TUPMP016.

[4] T. Yasui *et al.*, "J-PARC MR operation with the high repetition rate upgrade", *Proc. IPAC'23*, Venice, Italy, May 2023. pp. 1294-1298. doi:10.18429/JACoW-IPAC2023-TUXG1.

[5] T. Shimogawa *et al.*, "A control system of new magnet power converter for J-PARC main ring upgrade", *IEEE Trans. Nucl. Sci.*, vol. 66, no. 7, pp. 1236-1241, 2019. doi:10.1109/TNS.2019.2899380.

[6] C. Yamazaki *et al.*, "Beam acceleration experiment with developed 10 MW class high-precision power supply for accelerator electromagnets" *Proc. IPEC2010*, Sapporo, Japan, Jun. 2010. pp. 1526-1529. doi:10.1109/IPEC.2010.5544509.

[7] G. Fernqvist *et al.*, "Design and verification of a 24 kA calibration head for a DCCT test facility", *IEEE Trans. Instrum. Meas.*, 48 (2) (1999) 346-350. doi:10.1109/19.769598.